

Development of Collision Avoidance System in Slippery Road Conditions

Hwangjae Lee, Seibum Choi, *Member, IEEE*,

Abstract—This paper presents a path planning and tracking system optimized for collision avoidance on slippery roads. During path planning, a path that can induce the maximum possible lateral acceleration is generated through the fifth-order spline in consideration of the tire-road friction. The generated path is tracked based on the model predictive control (MPC), and the nonlinearity generated by the tire and low friction surface is reflected through the extended bicycle model and the combined brushed tire model. Inside the controller, a new type of yaw rate constraint considering sideslip angles is utilized to prevent the vehicle from becoming unstable on slippery roads and maximize lateral maneuver of the vehicle at the same time. The proposed system is verified by the vehicle dynamics software CarSim, and the simulation results show that it significantly increases the possibility of collision avoidance in slippery road conditions.

Index Terms—Path planning, Fifth-order spline, Model predictive control (MPC), Curvature optimization, Yaw rate constraint, Low- μ surface.

I. INTRODUCTION

OVER the past few years, as the types of recognition sensors installed in vehicles have become more diverse and their prices have become cheaper, the safety features of vehicles have developed rapidly [1], [2]. Functions such as lane keeping assist, lane change assist, and lane departure warning have already been commercialized to protect drivers from the risk of accidents [3], [4]. Going one step further, the evasive steering system provides a function to actively avoid the obstacle by manipulating the steering torque when an obstacle that cannot be avoided by braking alone is recognized [5]. These technologies go beyond the driver's driving assistance function and are applied to unmanned vehicles, making collision avoidance, one of the ultimate goals of autonomous driving, more feasible. Collision avoidance can be divided into path planning that generates collision-free trajectory and path tracking that follows the generated path as accurately as possible [6].

First, vehicle path planning for collision avoidance should reflect vehicle dynamics and non-holonomic characteristics, unlike path planning of robots and UAVs, which have been widely studied in the past. Studies on vehicle local path planning mainly use techniques such as spline curve and potential field [7], [8], [9], [10]. However, the studies mentioned above have a limitation in that they assume the road on which the vehicle travels in an ideal state for collision avoidance and generate a path that does not consider the frictional force

of the ground. Hu *et al.* [7] proposed a method of creating a path using cubic splines in consideration of obstacles and vehicle speed, but due to the characteristics of the cubic spline, sudden curvature change can inevitably occur, which makes the vehicle unstable on a road with low friction. Shim *et al.* [8] tried to create a path with the smoothest possible curvature by using the fifth-order spline, but it requires parameters that are difficult to obtain in real situations, such as steer angle, vehicle speed and vehicle acceleration at the final point. Chu *et al.* [9] tried to reflect the friction force between the ground surface and the tire to some extent by setting the path generation distance as a function of the speed and setting the speed as a variable that considers the maximum lateral acceleration. However, the maximum lateral acceleration is set heuristically, so there is a limit to reflect real-time road conditions. The potential field technique also uses the concepts of attractive and repulsive force to be suitable for local path generation, but a factor related to ground friction force is only the braking distance not the lateral movement [11].

Once a path is generated, the generated path can be tracked by various kinds of controllers [12]. Kapania *et al.* [13] used a feedforward-feedback controller and Guo *et al.* [14] used a sliding mode controller. Peng *et al.* [15] and Kim *et al.* [16] used MPC. Other types of controllers such as linear quadratic Gaussian controller and nonlinear adaptive controller have also been used [17], [18]. Considering the characteristic of path planning that the path of the future time step can be generated, the MPC taking the future reference into account is one of the good candidates as a tracker among the many types of controllers. In addition, as the vehicle's computational capability is improving, MPC has been receiving more choices as a tracking controller [19], [20], [21], [22]. However, despite the advantages of MPC's predictive characteristics, non-linearity in vehicle dynamics that inevitably occurs while driving on a slippery road can degrade the performance of MPC, so how to reflect such non-linearity in the controller is an important issue.

MPC can also handle constraints. This can be used as an important tool to maintain lateral stability of the vehicle. Rajamani [23] proposed a lateral acceleration bounding method through the appropriate yaw rate constraint to prevent excessive lateral acceleration that can make a vehicle unstable. Many studies have adopted this method to bound the maximum lateral acceleration [24], [25], [26], [27], [28]. However, this method has a limitation. It roughly approximates the effect of the sideslip angle and substitutes this value with the heuristic value, so that it does not fully reflect the mutual impact between yaw rate and sideslip angle.

Hwangjae Lee and Seibum Choi are with the Korea Advanced Institute of Science and Technology, Daejeon 34141, South Korea (e-mail: xexi7040@kaist.ac.kr; sbchoi@kaist.ac.kr).

In this paper, the collision avoidance system optimized on slippery roads is proposed by taking the above-mentioned issues into account. First, the fifth-order spline path planner considering the tire-road friction is designed. Since the spline consists of polynomials, the curvature of the generated path can be easily calculated. In addition, the curvature has a linear relationship with the yaw rate of the vehicle that is associated with the lateral acceleration. Due to these characteristics, a path that can induce the maximum possible lateral acceleration in a specific road condition can be generated. The generated path by the fifth-order spline can also induce the natural movement of the vehicle because the curvature can always be expressed with high-order polynomials. Additionally, the nonlinearity of the tire force saturation is addressed through the tire force linearization and the use of combined brushed tire model. Finally, the maximum lateral acceleration is bounded by utilizing the new type of yaw rate constraint inside the controller. It not only prevents the vehicle from becoming unstable but increases the ability of lateral maneuver. Each element of the system is organically connected to each other, and it helps the vehicle to avoid collisions on a slippery road.

The remainder of this paper is organized as follows. Section II briefly introduces the structure of the proposed system. In Section III, path planning strategy with the curvature optimization algorithm is introduced. In Section IV, the vehicle model that handles the nonlinearity is developed. Section V presents constructing the controllers in accordance with constraints. The performance of the system is verified by simulations in Section VI, and the paper is concluded in Section VII.

II. STRUCTURE OF THE SYSTEM

This section describes the overall architecture of the collision avoidance system. Fig. 1 shows the flow structure of the system consisting of the path planner, path tracker, and other signal processors.

In the path planner, the maximum lateral acceleration inducing path is generated while it is guaranteed to be collision-free through the proposed curvature optimization algorithm. The planner uses the signals measured from the vehicle and estimated from the observer. The path generated by the path planner is transmitted as a reference to the path tracker in the form of yaw rate r .

The path tracker is composed of the upper and the lower controller. The upper controller generates the required yaw moment M_z necessary to follow the reference yaw rate based on the MPC. The required yaw moment generated at this time means the additional yaw moment that reflects dynamics and non-linearity of the vehicle, excluding kinematic factors between steer angle δ_f and yaw rate. Additionally, the upper controller applies the switching mode constraint that combines two constraints so that the maximum lateral acceleration of the vehicle does not exceed a certain limitation value. In the lower controller of the path tracker, the steer angle corresponding to the required yaw moment is calculated using the tire force model. In order to utilize the tire model applied in this paper, the tire longitudinal stiffness parameter C_x , the tire lateral stiffness parameter C_α , and the tire-road friction coefficient μ are obtained through the tire model parameter identifier [29].

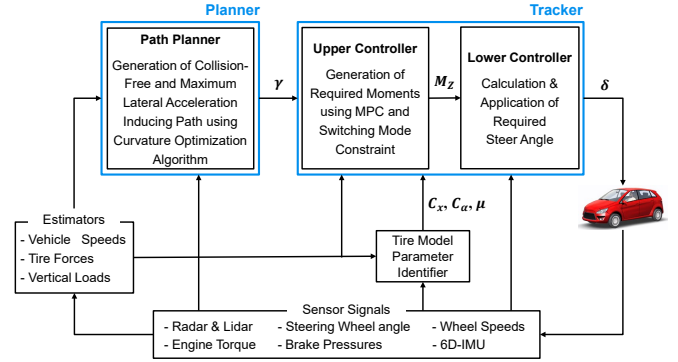


Fig. 1. Flow structure of the system.

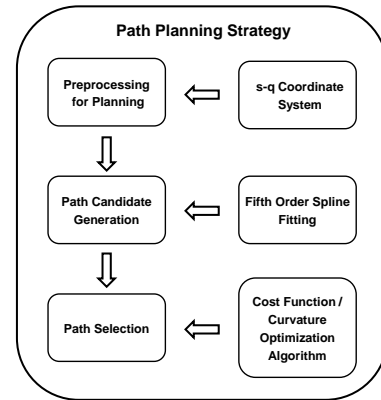


Fig. 2. Path planning strategy.

III. PATH PLANING

The purpose of the path planning is to create a path that can derive the physically possible maximum lateral acceleration to avoid obstacles on a low friction surface. As shown in Fig. 2, the path planning can be divided into three stages.

The first stage is the preprocessing stage for path planning, and it is the process of preparing data such as maps, vehicle positions, and heading angles to be applied to the s-q coordinate system. The s-q coordinate system can express the position of a vehicle as a distance from the waypoint s , and a lateral distance from the center line that connects waypoints q as shown in Fig. 3.

In the second stage, a number of path candidates are generated using fifth-order polynomials and boundary conditions based on the initial and final states of the vehicle.

In the final stage, the optimal collision-free trajectory is selected through the cost assessment of each generated path for safety, smoothness, and lane following. At the same time, considering the friction force between the road surface and the tire, it is determined whether the selected path can induce the maximum lateral acceleration. If not, the above steps are repeated until the collision-free trajectory that can induce the maximum lateral acceleration of the vehicle is found.

A. Preprocessing on s-q Coordinate System

In order to create a path using the s-q coordinate system, it is necessary to express the center line of the s-q coordinate

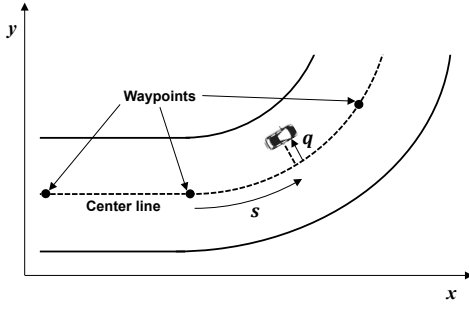


Fig. 3. s-q coordinate system.

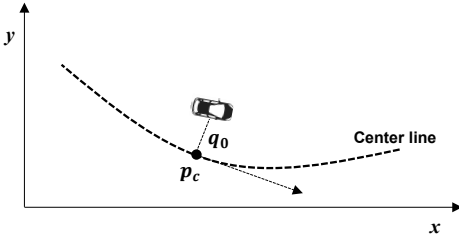


Fig. 4. Vehicle localization.

system as arc-length parameterized curves. Considering that global path planning is outside the scope of this paper, we assume the waypoints shown in Fig. 3 are given from a map. Then, the center line connecting the waypoints can be expressed as the following fifth-order polynomials using the arc length of the curve as a parameter [30]:

$$\begin{cases} x_c(s) = a_x s^5 + b_x s^4 + c_x s^3 + d_x s^2 + e_x s + f_x \\ y_c(s) = a_y s^5 + b_y s^4 + c_y s^3 + d_y s^2 + e_y s + f_y \end{cases} \quad (1)$$

where x_c and y_c are the Cartesian coordinates of the center line. Since the center line is parameterized with the arc length of the curve, the heading θ_c and curvature κ_c of the center line can be easily obtained with the first and second derivatives of the arc length parameterized fifth-order spline curves as follows [31]:

$$\theta_c = \arctan \frac{dy_c}{dx_c}, \quad \kappa_c = \frac{\dot{x}_c \ddot{y}_c - \ddot{x}_c \dot{y}_c}{(\dot{x}_c + \dot{y}_c)^{3/2}} \quad (2)$$

After expressing the center line as the arc-length parameterized curve, it is necessary to find out the position of the vehicle based on the center line to generate a path in the s-q coordinate system. As shown in Fig. 4, the distance between the vehicle and the center line q_0 and the point on the center line that minimizes it p_c are numerically calculated using quadratic minimization and Newton's method [32].

Finally, a coordinate system transformation is required from the s-q coordinate system to the Cartesian coordinate system for the vehicle to track the generated path in the real world. The generated path in the s-q coordinate system has a relationship with the Cartesian coordinate system in accordance with the arc length of the center line as follows [33]:

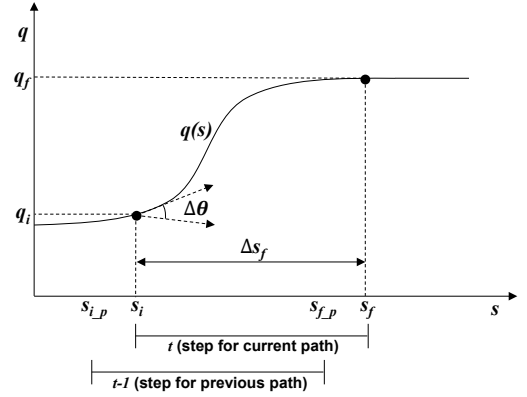


Fig. 5. Path candidate generation in the s-q coordinate system.

$$\frac{dx}{ds} = A \cos \theta, \quad \frac{dy}{ds} = A \sin \theta, \quad \frac{d\theta}{ds} = A \kappa \quad (3)$$

where x, y and θ are the position and orientation of the vehicle respectively, and κ is the curvature of the path that can be calculated as:

$$\kappa = \frac{B}{A} \left(\kappa_c + \left((1 - q\kappa_c) \left(\frac{d^2 q}{ds^2} \right) + \kappa_c \left(\frac{dq}{ds} \right)^2 \right) / A^2 \right) \quad (4)$$

with

$$A = \sqrt{\left(\frac{dq}{ds} \right)^2 + (1 - q\kappa_c)^2}, \quad B = \text{sgn}(1 - q\kappa_c) \quad (5)$$

This approach allows transformation between s-q coordinates and Cartesian coordinates.

B. Path Candidate Generation

The curvature of the path is determined by the curvature of the center line and the lateral offset q . In particular, the first and second derivatives of the lateral offset are also reflected in the curvature of the generated path as shown in (4). This means that the final driving path can be generated if only the lateral offset function is designed because the curvature of the center line is already determined by the global path and can be calculated. As shown in Fig. 5, the lateral offset function, which serves as a path candidate, is a function of the arc length in the s-q coordinate system and can be expressed as the fifth-order polynomial as follows:

$$q(s) = \begin{cases} a\Delta s^5 + b\Delta s^4 + c\Delta s^3 + d\Delta s^2 + e\Delta s + q_i, & s \in [s_i, s_f] \\ q_f, & \text{others} \end{cases} \quad (6)$$

where $\Delta s = s - s_i$. The first and second derivatives of the lateral offset function, other factors affecting the curvature of the path, are also expressed as:

$$\begin{aligned} \frac{dq}{ds}(s) &= \begin{cases} 5a\Delta s^4 + 4b\Delta s^3 + 3c\Delta s^2 + 2d\Delta s + e, & s \in [s_i, s_f] \\ 0, & \text{others} \end{cases} \\ \frac{d^2q}{ds^2}(s) &= \begin{cases} 20a\Delta s^3 + 12b\Delta s^2 + 6c\Delta s + 2d, & s \in [s_i, s_f] \\ 0, & \text{others} \end{cases} \end{aligned} \quad (7)$$

Since the lateral offset function has a total of six coefficients, at least six boundary conditions are required to determine all coefficients. First, the position of the current vehicle on the s - q coordinate system s_i and the lateral offset q_i that are shown in Fig. 5 are obtained in the preprocessing stage. The first derivative of the lateral offset function at s_i can be expressed as the tangent value of the angle difference $\Delta\theta$ that is defined by the difference between the vehicle heading angle and the tangent angle of the center line at the current position [34]. In addition, the second derivative of the lateral offset function at s_i can be expressed as a function of the curvature of the path using (4). Finally, since various types of paths can be created according to the settings of the arc length s_f and the lateral offset q_f at the final point, it can be set as design parameters according to the driving environment. For reference, $s_{i,p}$ and $s_{f,p}$ shown in Fig. 5 correspond to s_i and s_f respectively, and those are the values obtained in the previous step. Considering the above relationships, the boundary conditions for the fifth-order polynomial are as follows:

$$\begin{aligned} q(s_i) &= q_i, q(s_f) = q_f, \frac{dq}{ds}(s_i) = \tan \Delta\theta, \frac{dq}{ds}(s_f) = 0, \\ \frac{d^2q}{ds^2}(s_i) &= \frac{1}{(1 - qK_c)} \left(\frac{A^3 \kappa_p}{B} - \kappa_c \left(A^2 + \left(\frac{dq}{ds} \right)^2 \right) \right), \\ \frac{d^2q}{ds^2}(s_f) &= 0 \end{aligned} \quad (8)$$

where κ_p is the curvature at the starting point of the t -step calculated at the $t-1$ step in consideration of the vehicle speed, the acceleration, and the sampling time of the system.

With these six boundary conditions, all six coefficients in the fifth-order polynomial are determined, and the second derivative of the polynomial can also be expressed as a high-order polynomial. This ensures that the curvature of the generated path is continuous and smooth on every step.

In generating a number of path candidates, s_f and q_f mentioned above are important design parameters that determine the performance of the real-time path generation algorithm. s_f can be naturally derived by adding s_i to the distance of the lateral offset change Δs_f once it is determined. The method of determining Δs_f in this paper is closely related to the curvature optimization algorithm in path selection, so it will be discussed in detail in the next section.

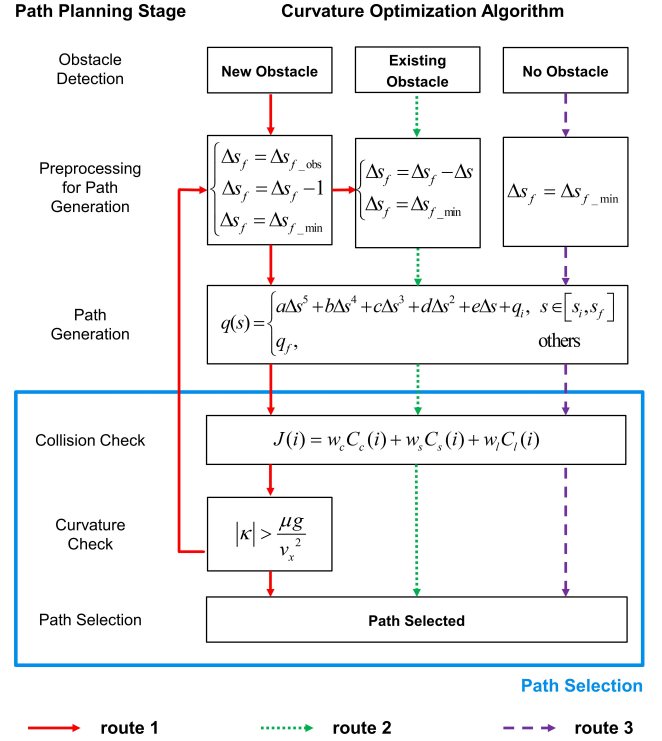


Fig. 6. Path selection flow chart.

q_f is a value that can be set in consideration of the range and the resolution of the lateral offset. In this study, considering the collision avoidance situation on a one-way two-lane road with a total road width of 8 m, the lateral offset of 6 m in each side and 12 m in total range is set. As the resolution of the lateral offset increases, the details of path generation also increase. However, it can also cause the computational complexity. Accordingly, the resolution of the lateral offset is experimentally set to 0.4 m, which is a resolution that can have sufficient performance for collision avoidance in this road condition without a huge computational burden. As a result, a total of thirty-one path candidates are created every step based on the above settings.

C. Path Candidate Generation

Among the thirty-one generated paths, the most optimal path that is collision-free and induces the maximum possible lateral acceleration can be selected as shown in Fig. 6. The selection process mainly consists of two parts; collision check and curvature check.

In the stage of collision check, the main purpose is to select a path minimizing three cost functions with each weighting factor. The three cost functions are about collision avoidance, consistency of path and lane following. The final cost function expressed as a linear sum of these is as follows:

$$J(i) = w_c C_c(i) + w_s C_s(i) + w_l C_l(i) \quad (9)$$

where i is the index of a path, C_c is the cost for the collision avoidance, C_s is the cost for the consistency of a path, and

C_l is the cost for the lane following. w_c , w_s , and w_l are the weighting factors for each of the costs mentioned above. For detailed algorithms on the elements of (9), [7] and [9] can be referred to.

In the curvature check stage, it is checked whether the candidate path has a curvature that can induce the maximum possible lateral acceleration considering the friction force between the tire and the road. Yaw rate of the vehicle is expressed by the following equation using the longitudinal speed of the vehicle v_x and the curvature of the tracking path:

$$\gamma = v_x \kappa \quad (10)$$

In addition, considering that the lateral acceleration of the vehicle is physically bounded based on the tire-road friction coefficient μ and the gravitational acceleration g and that the lateral acceleration is predominantly affected by the yaw rate as follows:

$$|a_y| \leq \mu g, \quad a_y \approx v_x \gamma \quad (11)$$

the curvature of the path inducing the maximum possible lateral acceleration can be bounded as a function of the tire-road friction coefficient, which is given by:

$$|\kappa| \leq \frac{\mu g}{v_x^2} \quad (12)$$

To summarize, it is possible to select a path with a curvature maximizing the lateral acceleration of the vehicle in a specific road condition by utilizing the fact that the curvature of the candidate path is bounded by the tire-road friction coefficient.

Unless the curvature of the generated path is the same as the curvature of the center line, the maximum absolute value of the curvature of the path increases as the distance of the lateral offset change decreases in the path generation stage. By utilizing these characteristics, the curvature optimization algorithm optimizes the curvature of the candidate path by changing Δs_f in the preprocessing stage. The algorithm divides a situation into three different cases according to the presence of a new obstacle as shown in Fig. 6. Although the main purpose of this algorithm is to select a path that induces maximum possible lateral acceleration, the algorithm itself is applied throughout the whole path planning stages.

First, if none of obstacle is recognized, a path is created and selected along route 3, and Δs_f is set to the default value of Δs_{f_min} in the preprocessing stage. Δs_{f_min} is the tunable minimum distance of the lateral offset change. The vehicle can quickly converge to the desired lane by setting Δs_f to Δs_{f_min} . In this case, there is no change in Δs_f , and no curvature optimization is performed.

On the other hand, when a new obstacle is recognized, a path is created and selected along route 1. The initial Δs_f is set to Δs_{f_obs} , and this value is the distance between the obstacle and the vehicle. However, if the maximum absolute value of the curvature of the collision-free candidate path does not satisfy the following equation after the collision check, Δs_f is reset to 1 m less in the preprocessing stage and starts to generate new candidate paths:

$$|\kappa| > \frac{\mu g}{v_x^2} \quad (13)$$

If it is confirmed that there is a path satisfying both the collision check and the curvature check through the iteration, the value of Δs_f one step before the last iteration is finally selected. By doing so, the path that is collision-free and has the largest curvature satisfying (12) can be obtained. Δs_f is then transferred to the preprocessing stage of route 2. In contrast, if the path already satisfies (13) without any iteration, Δs_f is set as Δs_{f_obs} , so that the path with the smallest curvature satisfying (13) is selected.

In route 1, one of the additional considerations is whether the vehicle must avoid the obstacle. The appearance of the new obstacle does not necessarily mean that the vehicle must avoid it. If there is no need to avoid the obstacle, such as a new obstacle in the opposite lane of the vehicle, the curvature of the candidate path may not change with the change of Δs_f . In this case, a final candidate path is set to pass the curvature check when Δs_f reaches Δs_{f_min} .

In route 2, Δs_f is continuously modified according to the moving distance of the vehicle so that the selected path to avoid the previously recognized obstacle matches the selected path in route 1 as much as possible. Also, abrupt manipulations that may occur when Δs_f is too short during the actual path following can be prevented by setting Δs_{f_min} . Δs_{f_min} is a tuning parameter and the value is experimentally determined as 20 m in the algorithm.

The curvature optimization algorithm is applied to the system through a rule-based method, and the finally selected path is transmitted to the controller as yaw rate references using (10).

IV. VEHICLE MODEL

When driving on a low friction surface, the tire force easily approaches the frictional limit showing many non-linear characteristics. In this section, a vehicle model is developed to reflect those nonlinearities.

A. Bicycle Model with Linearized Tire Forces

The bicycle model is suitable for representing the lateral behavior of a vehicle and the left and right wheels are lumped into the one wheel as shown in Fig. 7. Expressing the vehicle's lateral dynamics with the vehicle's side slip angle β and yaw rate as state variables is as follows:

$$\begin{aligned} m v_x (\dot{\beta} + \gamma) &= F_{yf} + F_{yr} \\ I_z \dot{\gamma} &= l_f F_{xf} - l_r F_{xr} + M_z \end{aligned} \quad (14)$$

where m is the vehicle mass; I_z is the vehicle yaw moment of inertia; M_z means the yaw moment; l_f and l_r denote the distances from the center of gravity to the front and rear axles; F_{yf} and F_{yr} represent the front and rear lateral tire force respectively. F_{yf} and F_{yr} can also be approximated as linear functions of tire slip angle as follows:

$$F_{yf} = C_f \alpha_f, \quad F_{yr} = C_r \alpha_r \quad (15)$$

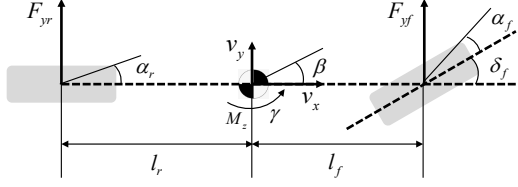


Fig. 7. Vehicle lateral dynamics model.

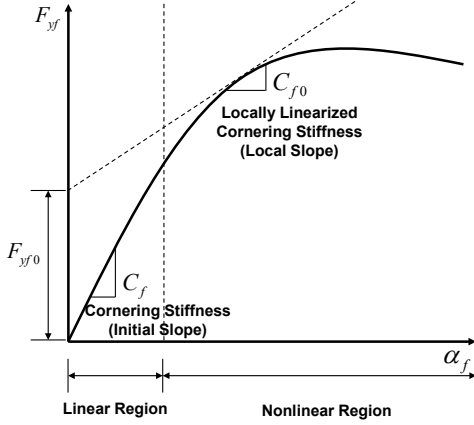


Fig. 8. Lateral tire force curve.

where C_f and C_r are the cornering stiffness of the front and rear tires; α_f and α_r are the tire slip angles of the front and rear tires respectively.

In particular, C_f and C_r mean the slope of the lateral tire force curve in the linear section as shown in Fig. 8. However, (15) generates a large error when the lateral tire force exhibits nonlinear characteristics. To reduce this error, if the lateral tire force curve is locally linearized with respect to the current operating point, the equations that can be applied to both the linear and non-linear regions are obtained as follows [35];

$$F_{yf} = C_{f0}\alpha_f + F_{yf0}, \quad F_{yr} = C_{r0}\alpha_r + F_{yr0} \quad (16)$$

where C_{f0} and C_{r0} are the slopes of the current α 's lateral tire force curve; F_{yf0} and F_{yr0} are the residual tire forces as shown in Fig. 8.

Considering that α_f and α_r have the following relations:

$$\alpha_f = \delta_f - \left(\beta + \frac{l_f \gamma}{v_x} \right), \quad \alpha_r = -\beta + \frac{l_r \gamma}{v_x} \quad (17)$$

the vehicle model that reflects the nonlinearity of tire force can be derived by combining equations (14)-(17), as follows:

$$\begin{aligned} \dot{x} &= Ax + B_\delta \delta_f + B_M M_z + E_{add} \\ y &= Cx \end{aligned} \quad (18)$$

where

$$\begin{aligned} x &= [\beta \quad \gamma]^T, \\ A &= \begin{bmatrix} -\frac{C_{f0} + C_{r0}}{I_z} & \frac{C_{r0}l_r - C_{f0}l_f}{I_z} - 1 \\ \frac{mv_x}{C_{r0}l_r - C_{f0}l_f} & -\frac{mv_x^2}{C_{f0}l_f^2 + C_{r0}l_r^2} \end{bmatrix}, B_\delta = \begin{bmatrix} \frac{C_{f0}}{I_z} \\ \frac{mv_x}{C_{f0}l_f} \end{bmatrix} \\ B_M &= \begin{bmatrix} 0 \\ \frac{1}{I_z} \end{bmatrix}, E_{add} = \begin{bmatrix} \frac{I_z v_x}{F_{yf0} + F_{yr0}} \\ \frac{mv_x}{l_f F_{yf0} - l_r F_{yr0}} \end{bmatrix}, C = \begin{bmatrix} 1 & 0 \\ 0 & 1 \end{bmatrix} \end{aligned} \quad (19)$$

B. Tire Model

The vehicle model derived in the previous section is modeled to reflect the nonlinearity of the tire force. In order to fully utilize it, a tire model that can express the nonlinearity of the tire is essential. Therefore, the following longitudinal and lateral combined brushed tire model, which can express tire nonlinearity close to reality, is applied [36], [37]:

$$F_{x,i} = \frac{C_x \left(\frac{\lambda_i}{1+\lambda_i} \right)}{f_i} F_i, \quad F_{y,i} = -\frac{C_\alpha \left(\frac{\tan \alpha_i}{1+\lambda_i} \right)}{f_i} F_i \quad (20)$$

where

$$\begin{aligned} F_i &= \begin{cases} f_i - \frac{1}{3\mu F_{z,i}} f_i^2 + \frac{1}{27\mu^2 F_{z,i}^2} f_i^3, & \text{if } f_i \leq 3\mu F_{z,i} \\ \mu F_{z,i}, & \text{otherwise} \end{cases} \\ f_i &= \sqrt{C_x^2 \left(\frac{\lambda_i}{1+\lambda_i} \right)^2 + C_\alpha^2 \left(\frac{\tan \alpha_i}{1+\lambda_i} \right)^2} \end{aligned} \quad (21)$$

In (20) and (21), F_z is the tire normal force; λ_i and α_i are the slip ratio and the slip angle of the i th wheel where $i = 1,2,3,4$ which correspond to the left-front, right-front, left-rear, and right-rear wheels respectively. In addition to the measurable parameters by the sensors, C_x , C_α , and μ are also identified by the linearized recursive least square method [29].

When all parameters are determined in this way, the lateral tire force curve for α can be drawn by setting other variables except α as constants. Finally, the required parameters for the vehicle model such as C_{f0} , C_{r0} , F_{yf0} , and F_{yr0} can be obtained by locally linearizing the lateral tire force curve at the operating point.

V. DESIGN OF CONTROLLERS

The path finally selected in the path planner is transmitted to the path tracker in the form of the vehicle's yaw rate required to track the path. This path tracker is composed of the upper and lower controllers. The upper controller calculates the yaw moment required to generate the reference yaw rate, and the lower controller applies the additional steering necessary to realize the required yaw moment to the vehicle. This section describes the two controllers of the path tracker.

A. Upper Controller

The upper controller of the path tracker is composed of MPC that determines the optimal control input of the current step in consideration of future references. In particular, the switching mode constraint, which changes the constraint according to the situation, is applied in the MPC to prevent the vehicle from becoming unstable due to the low tire-road friction and at the same time to enable the maximum possible lateral movement.

1) *MPC formulation*: To formulate the MPC, the bicycle model with linearized tire forces (18), is discretized using zero-order hold as follows:

$$\begin{aligned} x_d(k+1) &= A_d x_d(k) + B_{M-d} u(k) + E_d(k) \\ y_d(k) &= C_d x_d(k) \end{aligned} \quad (22)$$

where

$$\begin{aligned} E_d(k) &= B_{\delta-d} \delta_{f-d}(k) + E_{add-d} \\ u(k) &= M_{z-d}(k) \end{aligned} \quad (23)$$

Subscript d stands for discrete vector or matrix, and k stands for k th step in discrete time. In $E_d(k)$, $\delta_{f-d}(k)$ can be set as a time-varying variable through the following relation using the reference yaw rate generated from the path, and the remaining terms are made constant over the prediction time span:

$$\delta_f = \frac{L}{V_x} \gamma \quad (24)$$

where L is the front-rear axle distance.

In the next step, the system model in (22) is augmented to obtain Δu as the manipulated variable for the output of the controller as follows [38]:

$$\begin{aligned} x_a(k+1) &= A_a x_a(k) + B_a \Delta u(k) + E_a \Delta e(k) \\ y_a(k) &= C_a x_a(k) \end{aligned} \quad (25)$$

where

$$\begin{aligned} x_a(k+1) &= \begin{bmatrix} \Delta x_d(k+1) \\ y_d(k+1) \end{bmatrix}, A_a = \begin{bmatrix} A_d & O \\ C_d A_d & I \end{bmatrix} \\ B_a &= \begin{bmatrix} B_d \\ C_d B_d \end{bmatrix}, E_a = \begin{bmatrix} I \\ C_d \end{bmatrix}, C_a = [O \quad I] \\ \Delta x_d(k) &= x_d(k) - x_d(k-1) \\ \Delta u(k) &= u(k) - u(k-1) \\ \Delta e(k) &= E_d(k) - E_d(k-1) \end{aligned} \quad (26)$$

One of the biggest features of MPC is to predict future output through the model using the information of current state variables. Therefore, based on the above model, the future output variables Y can be explicitly expressed as the current state variables $x_a(k)$, the future control parameters ΔU , and the future extra terms ΔE as follows:

$$Y = F x_a(k) + G \Delta U + H \Delta E \quad (27)$$

where each component is expressed in (28)

In (28), N_p and N_c are the prediction horizon and the control horizon respectively. N_c normally can be set equal

to or less than N_p . In this controller, N_p is set as 50 while N_c is set as 10.

The final goal of the upper controller is to most closely match the vehicle's yaw rate predicted from the MPC with the reference yaw rate, so define a cost function reflecting this control goal as follows:

$$J = (R_{ref} - Y)^T Q (R_{ref} - Y) + \Delta U^T R \Delta U \quad (29)$$

where

$$R_{ref} = \begin{bmatrix} \beta_{ref}(k+1) \\ \gamma_{ref}(k+1) \\ \vdots \\ \beta_{ref}(k+N_p) \\ \gamma_{ref}(k+N_p) \end{bmatrix}, Y = \begin{bmatrix} \beta(k+1) \\ \gamma(k+1) \\ \vdots \\ \beta(k+N_p) \\ \gamma(k+N_p) \end{bmatrix} \quad (30)$$

$$Q = \text{blockdiag}\{W, \dots, W\}, R = \text{blockdiag}\{I, \dots, I\}$$

$$W = \text{diag}\{0, 1\}, I = \text{diag}\{1, 1\}$$

In (29), subscript *ref* stands for a reference.

2) *Constraint analysis for MPC*: In the absence of bounding for the vehicle's lateral acceleration, the vehicle's tire force can easily saturate on a low friction surface, leading to unstable vehicle behavior. To prevent such unstable behavior, constraints can be applied to the lateral acceleration. The lateral acceleration at the center of gravity of the vehicle is given by:

$$a_y = v_x \gamma + \tan(\beta) \dot{v}_x + \frac{v_x \dot{\beta}}{\sqrt{1 + \tan^2(\beta)}} \quad (31)$$

Since the side slip angle of a vehicle is generally a small value, the small-angle approximation is applicable. Moreover, it is difficult to make a sudden change in the longitudinal speed on a slippery road. Taking these into account, (31) is concisely expressed as follows:

$$a_y = v_x \gamma + v_x \dot{\beta} \quad (32)$$

By combining (32) with (11) that means the lateral acceleration is physically bounded by the tire-road friction coefficient, the yaw rate can be bounded as follows:

$$-0.85 \frac{\mu g}{v_x} - \dot{\beta} \leq \gamma \leq 0.85 \frac{\mu g}{v_x} - \dot{\beta} \quad (33)$$

0.85 can be adjusted according to the amount of lateral acceleration to be bounded.

It should be noted that when the signs of λ and $\dot{\beta}$ are different, the yaw rate can be maximized at the same time the maximum lateral acceleration is bounded. This means more lateral maneuver. On the other hand, when the signs of λ and $\dot{\beta}$ are the same, the maximum lateral acceleration is bounded to the same value, while the yaw rate may represent a relatively small value. This conversely means less lateral maneuver. To summarize, given the same lateral acceleration, more lateral maneuver is possible when the yaw rate is larger. By utilizing this concept with the conventional yaw rate bounding method [23], the following switching mode constraint can be constructed:

$$\begin{cases} -0.85 \frac{\mu g}{v_x} - \dot{\beta} \leq \gamma \leq 0.85 \frac{\mu g}{v_x} - \dot{\beta}, & \text{if } \text{sgn}(\gamma) \neq \text{sgn}(\dot{\beta}) \\ -0.85 \frac{\mu g}{v_x} \leq \gamma \leq 0.85 \frac{\mu g}{v_x}, & \text{otherwise} \end{cases} \quad (34)$$

This type of constraints has the effect of maximizing the yaw rate when the signs of λ and $\dot{\beta}$ are different while maintaining the same limit of maximum lateral acceleration.

The upper controller computes the cost function (29), subjects to (27) and (34) through the quadratic programming to obtain the optimized ΔU .

B. Lower Controller

Since the yaw moment from the upper controller is the required additional yaw moment compared to the steering input from (24), the lower controller calculates the steer angle to be applied to the vehicle in consideration of this. First, the required tire lateral force F_{y_req} to generate the required yaw moment can be obtained as follows:

$$F_{y_req} = \frac{M_z}{2l_f} \quad (35)$$

If the F_{y_req} is added to the current lateral force F_{y1} as shown in Fig. 9, the target lateral force F_{y2} is obtained. Because the lateral tire force curve can be plotted through the tire model developed in the previous section, the target slip angle α_2 corresponding to the target lateral force can also be obtained.

Finally, using the relationship between a steer angle and a slip angle (17), the target steer angle to be applied to the vehicle δ_{f_tar} is computed as follows:

$$\delta_{f_tar} = \delta_f + \left(\beta + \frac{l_f}{v_x} \gamma - \alpha_2 \right) \quad (36)$$

In addition, the max value of α , α_{max} , is set so that α_2 does not exceed α_{max} to prevent the tire force from decreasing in the nonlinear region as shown in Fig. 9.

VI. SIMULATION ANALYSIS

The performance of the proposed collision avoidance system was evaluated using the front-wheel driving B-class hatchback model in the high-fidelity simulation software, CarSim. As a scenario for simulation, two vehicles are located in front of the host vehicle as shown in Fig. 10, so a double lane change is required to completely avoid a collision. In order to depict a situation requiring the most urgent lateral maneuver, the obstacle vehicles are considered to have a zero longitudinal speed. The tire-road friction coefficient is 0.3 similar to the friction coefficient of a snow-covered road, and the host vehicle's initial speed is 20 m/s. Considering the vehicle's sensor detection range which is 60 m in this simulation, it is impossible to avoid the collision by braking alone because the minimum breaking distance with the anti-lock braking system (ABS) is beyond the maximum sensing distance.

There is no limit for the detection sensors of the host vehicle to recognize the first obstacle vehicle as soon as it comes within the sensor detection range. However, it is usually difficult to recognize a vehicle in the opposite lane when there is another vehicle right in front because of the limitation of sensor detection angle. Taking this into consideration, the second obstacle vehicle is set to be detected by the sensors once the main body of the host vehicle passes to the second lane. The width of the host vehicle and the obstacle vehicles is assumed to be the same as 2 m, and the sampling time of the path planner and the tracker in the simulation is the same as 10 ms.

A. Comparison with Cubic Spline Path Planner

Prior to the overall system performance evaluation, it is noteworthy that the path planning using the fifth-order polynomial has advantages over the using the conventional cubic spline. Fig. 11 shows the paths and the curvatures of the paths generated by the fifth-order and the cubic spline planner to avoid the first obstacle vehicle. There is no significant difference when looking only at the generated paths, but there

$$\begin{aligned} Y &= \begin{bmatrix} y_a(k+1) & y_a(k+2) & y_a(k+3) & \cdots & y_a(k+N_p) \end{bmatrix}^T \\ F &= \begin{bmatrix} C_a A_a & C_a A_a^2 & C_a A_a^3 & \cdots & C_a A_a^{N_p} \end{bmatrix}^T \\ G &= \begin{bmatrix} C_a B_a & 0 & 0 & \cdots & 0 \\ C_a A_a B_a & C_a B_a & 0 & \cdots & 0 \\ C_a A_a^2 B_a & C_a A_a B_a & C_a B_a & \cdots & 0 \\ \vdots & \vdots & \vdots & \ddots & \vdots \\ C_a A_a^{N_p-1} B_a & C_a A_a^{N_p-2} B_a & C_a A_a^{N_p-3} B_a & \cdots & C_a A_a^{N_p-N_c} B_a \end{bmatrix} \\ \Delta U &= \begin{bmatrix} \Delta u(k) & \Delta u(k+1) & \Delta u(k+2) & \cdots & \Delta u(k+N_c-1) \end{bmatrix}^T \\ H &= \begin{bmatrix} C_a E_a & 0 & 0 & \cdots & 0 \\ C_a A_a E_a & C_a E_a & 0 & \cdots & 0 \\ C_a A_a^2 E_a & C_a A_a E_a & C_a E_a & \cdots & 0 \\ \vdots & \vdots & \vdots & \ddots & \vdots \\ C_a A_a^{N_p-1} E_a & C_a A_a^{N_p-2} E_a & C_a A_a^{N_p-3} E_a & \cdots & C_a E_a \end{bmatrix} \\ \Delta E &= \begin{bmatrix} \Delta e(k) & \Delta e(k+1) & \Delta e(k+2) & \cdots & \Delta e(k+N_p-1) \end{bmatrix}^T \end{aligned} \quad (28)$$

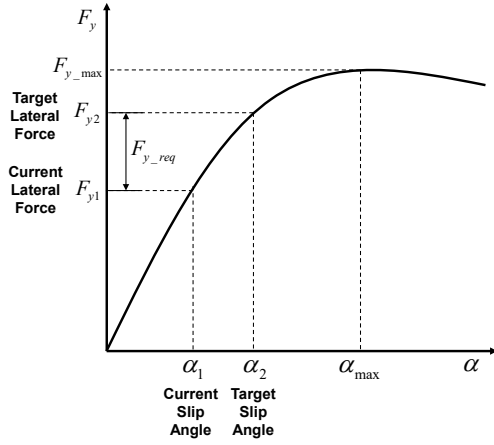


Fig. 9. Lateral tire force curve for the lower controller.

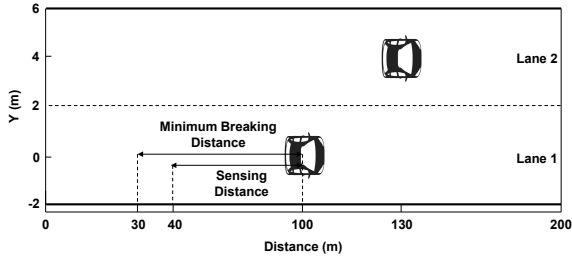


Fig. 10. Collision avoidance scenario.

is a big difference when looking at the curvatures of the paths. Basically, the curvature of the cubic spline shows a figure of a first-order polynomial while the curvature of the fifth-order spline shows a figure of a third-order polynomial. This is because the curvature of the path is dominantly determined by the second derivative of the polynomial representing the path in general.

It can be noted that the fifth-order spline planner creates a path close to the human-like driving path by comparing Fig. 12, which shows the single-lane change path and its curvature generated by the driver model, with Fig. 11. Accordingly, the path generated by the fifth-order spline planner creates a reference more suitable for the actual vehicle to track and it can prevent sudden and unnatural steering manipulations that can be caused from the path generated by the cubic spline planner.

B. Evaluation of the Collision Avoidance System

In order to specifically prove the performance of the curvature optimization algorithm and the switching mode constraint in the proposed collision avoidance system, simulations for three types of system including different control strategies as shown in Table. I were conducted. For Δs_f optimization, the curvature optimization algorithm and the method proposed by [9] were used. This method sets Δs_f as the function of the longitudinal speed of the vehicle with a linear design parameter k_v as shown in Type 3 in Table. I. As a method of limiting lateral acceleration, the switching mode constraint

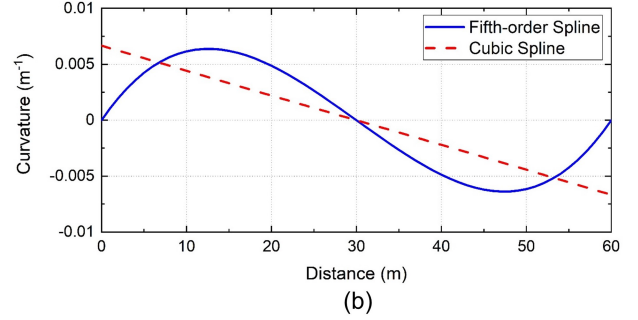
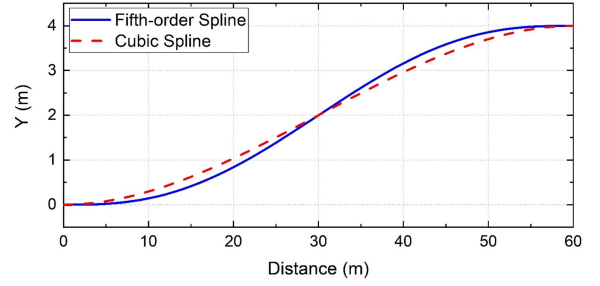


Fig. 11. Path and curvature of the path by fifth-order spline and cubic spline. (a) Path. (b) Curvature.

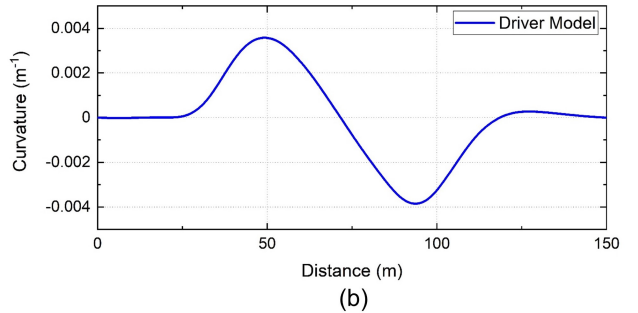
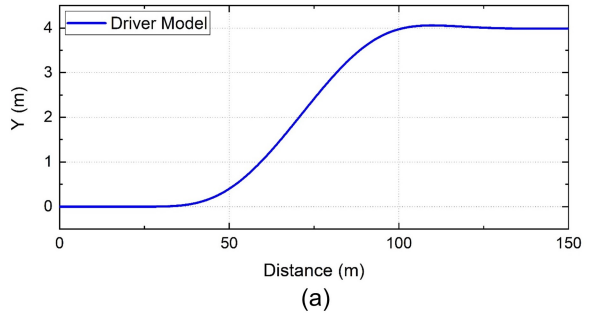


Fig. 12. Path and curvature of the path by driver model. (a) Path. (b) Curvature.

TABLE I
SYSTEM TYPES WITH DIFFERENT CONTROL STRATEGIES.

Type	Δs Optimization	Lateral Acceleration
Type1	Curvature Optimization Algorithm	Switching Mode Constraint
Type2	Curvature Optimization Algorithm	$ \gamma \leq 0.85 \frac{\mu g}{v_x}$
Type3	$\Delta s_f = k_v v_x + \Delta s_{\min}$	$ \gamma \leq 0.85 \frac{\mu g}{v_x}$

was applied to Type 1 and the widely used method [23] was applied to Type 2 and Type 3.

The overall simulation results are shown in Fig. 13. For

clarity, Fig. 13(a) plots the first reference yaw rate $\gamma_{ref}(k+1)$ at each time step out of the whole set. It is noted from Fig. 13(a) and (b) that the path planner of Type 1 and Type 2 can generate the reference yaw rate inducing the almost maximum lateral acceleration that can possibly occur on the road with the friction coefficient of 0.3 through the curvature optimization algorithm. On the other hand, the path planner of Type 3 generates the reference yaw rate yielding the lower lateral acceleration than the maximum lateral acceleration that the vehicle can generate by not considering the friction force of the surface.

When the host vehicle almost changed its lane from Lane 1 to Lane 2, the second obstacle vehicle in Lane 2 is newly detected causing the abrupt reference change to the host vehicle. In this moment, the path planner of Type 1 and Type 2 first sets Δs_f as Δs_{f_obs} but Δs_f does not decrease anymore since it finds that the curvature of the collision free path is already beyond the limit. In this situation, the path planner of Type 1 and Type 2 can successfully generate the smallest possible reference yaw rate that guarantees both the maximum lateral acceleration and being collision-free. On the

contrary, the path planner of Type 3 cannot properly respond to the second obstacle vehicle and keeps producing a reference that does not derive the maximum lateral acceleration of the vehicle.

In Fig. 13(c), the performance of the switching mode constraint in the MPC can be verified. First of all, note that the constraint of the conventional yaw rate indicated by the black dots in the graph tends to increase slightly over time as the vehicle's longitudinal speed naturally decelerates as shown in Fig. 13(d). The generated yaw rates of Type 2 and Type 3 stay within the constraint boundary and obviously cannot go beyond this boundary.

However, the switching mode constraint indicated by the pink short dots enables the boundary where the higher yaw rate can be generated regardless of the conventional yaw rate constraint when the signs of γ and $\dot{\beta}$ are opposite. When the sign of γ and $\dot{\beta}$ are the same in which the yaw rate constraint considering $\dot{\beta}$ is not beneficial the switching mode constraint sticks with the conventional yaw rate constraint. Accordingly, Type 1 can allow the higher yaw rate that cannot be allowed in Type 2 and Type 3 by using the extended boundary. It is

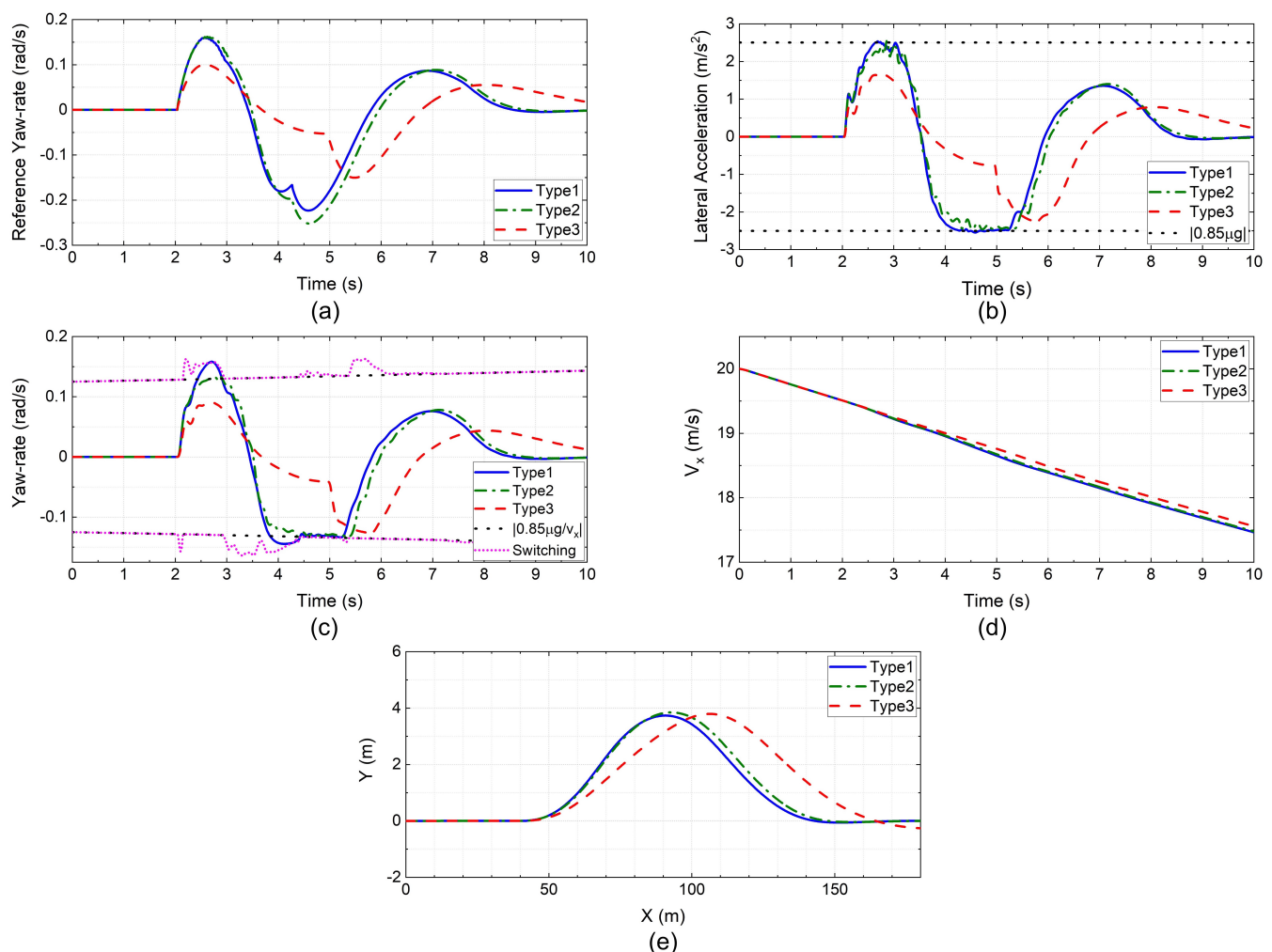


Fig. 13. Simulation results of the collision avoidance system in the slippery road condition. (a) Reference yaw rate. (b) Lateral acceleration. (c) Yaw rate. (d) Longitudinal velocity. (e) Trajectory.

TABLE II
COLLISION AVOIDANCE EFFICIENCY.

Assessment	Type1	Type2	Type3
Lateral Deviation	3.48 m	3.26 m	1.71 m
Relative Ratio	100 %	93.6 %	49.1 %

also noteworthy that even though the yaw rate of Type 1 is sometimes beyond the conventional yaw rate constraint, the maximum lateral acceleration of Type 1 is well bounded by the same lateral acceleration constraint as Type 2 and Type 3.

Finally, the trajectory to avoid the obstacle vehicles is shown in Fig. 13(e). In the case of Type 3, the first obstacle vehicle can be avoided with the relatively low lateral acceleration, but the second obstacle vehicle detected later cannot be completely avoided and the collision happens (Simulation proceeded to the end, assuming no collisions for comparison of results). On the other hand, Type 2 uses the maximum lateral acceleration to avoid the first obstacle vehicle and attempts to change lanes as quickly as possible. Consequently, it finds the second obstacle early, and returns to the original lane again using the maximum lateral acceleration. In the end, it successfully avoids both the first and second obstacle vehicles. Type 1 shows the lateral acceleration profile similar to that of Type 2, but it can be confirmed that the first and second obstacle vehicle can be avoided earlier than Type 2 because the generated yaw rate is relatively larger.

For objective comparison, Table. II shows the lateral distance between the host vehicle and the second obstacle vehicle at the moment of avoiding it and their relative ratio based on Type 1. Basically, Type 1 and Type 2 with the curvature optimization algorithm avoid the obstacles by securing almost double the inter-vehicle distance than Type 3 that uses the different Δs_f setting method. In addition, Type 1 with the switching mode constraint was able to secure about 7% more compared to Type2 that uses the conventional yaw rate constraint.

VII. CONCLUSION

In this paper, the overall collision avoidance system including the path planner and tracker that are specialized on slippery roads was developed and evaluated in the Carsim simulation environment. The proposed system highlights the following unique points from the previously reported methods: (1) The curvature of the path made of the fifth-order spline during the path planning shows at least a figure of third or higher order polynomials. It means that the generated path can be tracked with the steering that is very close to the actual human driving; (2) The path inducing the maximum lateral acceleration that the vehicle can physically produce is generated through the curvature optimization algorithm in the path planner by considering the friction force between the ground surface and tire; (3) The tire nonlinearity, which often appears on slippery roads during path tracking, is reflected through the extension of the bicycle model and the application of the combined brushed tire model. (4) For lateral acceleration bounding, the switching mode constraint combining the yaw rate constraint taking β into account and the conventional yaw

rate constraint is applied in MPC. It allows producing the higher yaw rate within the same lateral acceleration boundary compared to the conventional method. The simulation results of the system show that the proposed algorithms can control the vehicle to reliably avoid obstacles on the roads with low tire-road friction.

ACKNOWLEDGMENT

This research was partly supported by the BK21+ program through the NRF funded by the Ministry of Education of Korea; the Technology Innovation Program (20010263, Development of innovative design for UX environment improvement and commercialization model of wheelchair electric motorization kit with enhanced portability and convenience) funded By the Ministry of Trade, Industry Energy (MOTIE, Korea); the grant (20TLRP-C152478-02) from Transportation Logistics Research Program funded by Ministry of Land, Infrastructure and Transport (MOLIT) of Korea government and Korea Agency for Infrastructure Technology Advancement (KAIA); the National Research Foundation of Korea (NRF) grant funded by the Korea government (MSIP) (No. 2020R1A2B5B01001531); the Technology Innovation Program (20014983, Development of autonomous chassis platform for a modular vehicle) funded By the Ministry of Trade, Industry Energy (MOTIE, Korea).

REFERENCES

- [1] S. A. Bagloee, M. Tavana, M. Asadi, and T. Oliver, "Autonomous vehicles: challenges, opportunities, and future implications for transportation policies," *Journal of modern transportation*, vol. 24, no. 4, pp. 284–303, 2016.
- [2] K. Bengler, K. Dietmayer, B. Farber, M. Maurer, C. Stiller, and H. Winner, "Three decades of driver assistance systems: Review and future perspectives," *IEEE Intelligent transportation systems magazine*, vol. 6, no. 4, pp. 6–22, 2014.
- [3] J. Zhou and H. Peng, "Range policy of adaptive cruise control vehicles for improved flow stability and string stability," *IEEE Transactions on intelligent transportation systems*, vol. 6, no. 2, pp. 229–237, 2005.
- [4] C. Hu, Z. Wang, Y. Qin, Y. Huang, J. Wang, and R. Wang, "Lane keeping control of autonomous vehicles with prescribed performance considering the rollover prevention and input saturation," *IEEE transactions on intelligent transportation systems*, vol. 21, no. 7, pp. 3091–3103, 2019.
- [5] T. Hestermeyer, W. Bongarth, and J. Dornhege, "Steering features of the new ford focus," in *9th International Munich Chassis Symposium 2018*. Springer, 2019, pp. 487–504.
- [6] H. Wang and B. Liu, "Path planning and path tracking for collision avoidance of autonomous ground vehicles," *IEEE Systems Journal*, 2021.
- [7] X. Hu, L. Chen, B. Tang, D. Cao, and H. He, "Dynamic path planning for autonomous driving on various roads with avoidance of static and moving obstacles," *Mechanical Systems and Signal Processing*, vol. 100, pp. 482–500, 2018.
- [8] T. Shim, G. Adireddy, and H. Yuan, "Autonomous vehicle collision avoidance system using path planning and model-predictive-control-based active front steering and wheel torque control," *Proceedings of the Institution of Mechanical Engineers, Part D: Journal of automobile engineering*, vol. 226, no. 6, pp. 767–778, 2012.
- [9] K. Chu, M. Lee, and M. Sunwoo, "Local path planning for off-road autonomous driving with avoidance of static obstacles," *IEEE transactions on intelligent transportation systems*, vol. 13, no. 4, pp. 1599–1616, 2012.
- [10] R. Lemos, O. Garcia, and J. V. Ferreira, "Local and global path generation for autonomous vehicles using splines," *Ingenieria*, vol. 21, no. 2, pp. 188–200, 2016.
- [11] J. Ji, A. Khajepour, W. W. Melek, and Y. Huang, "Path planning and tracking for vehicle collision avoidance based on model predictive control with multiconstraints," *IEEE Transactions on Vehicular Technology*, vol. 66, no. 2, pp. 952–964, 2016.

- [12] Q. Yao, Y. Tian, Q. Wang, and S. Wang, "Control strategies on path tracking for autonomous vehicle: State of the art and future challenges," *IEEE Access*, vol. 8, pp. 161 211–161 222, 2020.
- [13] N. R. Kapania and J. C. Gerdes, "An autonomous lanekeeping system for vehicle path tracking and stability at the limits of handling," in *Proceedings of the 12th International Symposium on Advanced Vehicle Control (AVEC)*, 2014, pp. 720–725.
- [14] J. Guo, Y. Luo, and K. Li, "Adaptive neural-network sliding mode cascade architecture of longitudinal tracking control for unmanned vehicles," *Nonlinear Dynamics*, vol. 87, no. 4, pp. 2497–2510, 2017.
- [15] H. Peng, W. Wang, Q. An, C. Xiang, and L. Li, "Path tracking and direct yaw moment coordinated control based on robust mpc with the finite time horizon for autonomous independent-drive vehicles," *IEEE Transactions on Vehicular Technology*, vol. 69, no. 6, pp. 6053–6066, 2020.
- [16] E. Kim, J. Kim, and M. Sunwoo, "Model predictive control strategy for smooth path tracking of autonomous vehicles with steering actuator dynamics," *International Journal of Automotive Technology*, vol. 15, no. 7, pp. 1155–1164, 2014.
- [17] K. Lee, S. Jeon, H. Kim, and D. Kum, "Optimal path tracking control of autonomous vehicle: Adaptive full-state linear quadratic gaussian (lqg) control," *IEEE Access*, vol. 7, pp. 109 120–109 133, 2019.
- [18] P. Petrov and F. Nashashibi, "Modeling and nonlinear adaptive control for autonomous vehicle overtaking," *IEEE Transactions on Intelligent Transportation Systems*, vol. 15, no. 4, pp. 1643–1656, 2014.
- [19] H. Li and Y. Luo, "Integrated coordination control for distributed drive electric vehicle trajectory tracking," *International Journal of Automotive Technology*, vol. 21, no. 4, pp. 1047–1060, 2020.
- [20] H. Guo, D. Cao, H. Chen, Z. Sun, and Y. Hu, "Model predictive path following control for autonomous cars considering a measurable disturbance: Implementation, testing, and verification," *Mechanical Systems and Signal Processing*, vol. 118, pp. 41–60, 2019.
- [21] H. Guo, C. Shen, H. Zhang, H. Chen, and R. Jia, "Simultaneous trajectory planning and tracking using an mpc method for cyber-physical systems: A case study of obstacle avoidance for an intelligent vehicle," *IEEE Transactions on Industrial Informatics*, vol. 14, no. 9, pp. 4273–4283, 2018.
- [22] B. Zhang, C. Zong, G. Chen, and B. Zhang, "Electrical vehicle path tracking based model predictive control with a laguerre function and exponential weight," *IEEE Access*, vol. 7, pp. 17 082–17 097, 2019.
- [23] R. Rajamani, *Vehicle dynamics and control*. Springer Science & Business Media, 2011.
- [24] T. Ahn, Y. Lee, and K. Park, "Design of integrated autonomous driving control system that incorporates chassis controllers for improving path tracking performance and vehicle stability," *Electronics*, vol. 10, no. 2, p. 144, 2021.
- [25] B. Huang, S. Wu, S. Huang, and X. Fu, "Lateral stability control of four-wheel independent drive electric vehicles based on model predictive control," *Mathematical Problems in Engineering*, vol. 2018, 2018.
- [26] L. Xiong, G. Teng, Z. Yu, W. Zhang, and Y. Feng, "Novel stability control strategy for distributed drive electric vehicle based on driver operation intention," *International journal of automotive technology*, vol. 17, no. 4, pp. 651–663, 2016.
- [27] J. Feng, S. Chen, and Z. Qi, "Coordinated chassis control of 4wd vehicles utilizing differential braking, traction distribution and active front steering," *IEEE Access*, vol. 8, pp. 81 055–81 068, 2020.
- [28] K. Han, G. Park, G. S. Sankar, K. Nam, and S. B. Choi, "Model predictive control framework for improving vehicle cornering performance using handling characteristics," *IEEE Transactions on Intelligent Transportation Systems*, vol. 22, no. 5, pp. 3014–3024, 2020.
- [29] M. Choi, J. J. Oh, and S. B. Choi, "Linearized recursive least squares methods for real-time identification of tire–road friction coefficient," *IEEE Transactions on Vehicular Technology*, vol. 62, no. 7, pp. 2906–2918, 2013.
- [30] H. Wang, J. Kearney, and K. Atkinson, "Arc-length parameterized spline curves for real-time simulation," in *Proc. 5th International Conference on Curves and Surfaces*, vol. 387396, 2002.
- [31] I. N. Bronshtein and K. A. Semendiyayev, *Handbook of mathematics*. Springer Science & Business Media, 2013.
- [32] H. Wang, J. Kearney, and K. Atkinson, "Robust and efficient computation of the closest point on a spline curve," in *Proceedings of the 5th International Conference on Curves and Surfaces*, 2002, pp. 397–406.
- [33] T. D. Barfoot and C. M. Clark, "Motion planning for formations of mobile robots," *Robotics and Autonomous Systems*, vol. 46, no. 2, pp. 65–78, 2004.
- [34] B. Siciliano, L. Sciavicco, L. Villani, and G. Oriolo, "Modelling, planning and control," *Advanced Textbooks in Control and Signal Processing*. Springer, 2009.
- [35] M. Choi and S. B. Choi, "Model predictive control for vehicle yaw stability with practical concerns," *IEEE Transactions on Vehicular Technology*, vol. 63, no. 8, pp. 3539–3548, 2014.
- [36] H. Pacejka, *Tire and vehicle dynamics*. Elsevier, 2005.
- [37] Y.-H. J. Hsu, *Estimation and control of lateral tire forces using steering torque*. Stanford University, 2009.
- [38] L. Wang, *Model predictive control system design and implementation using MATLAB®*. Springer Science & Business Media, 2009.



Hwangjae Lee received the B.S. degree in weapons engineering from Korea Military Academy, Seoul, Korea, and M.S. in Mechanical Engineering from University of Wisconsin-Milwaukee, WI, USA, in 2009 and 2017 respectively. Since 2020, he is currently pursuing the Ph.D. degree in Mechanical engineering at Korea Advanced Institute of Science and Technology (KAIST). His research interests include vehicle dynamics and control, path planning, and active safety systems.



Seibum Choi (M'09) received the B.S. in mechanical engineering from Seoul National University, Seoul, Korea, the M.S. in mechanical engineering from KAIST, Daejeon, Korea, and the Ph.D. in control from the University of California, Berkeley, CA, USA, in 1993. From 1993 to 1997, he was involved in the development of automated vehicle control systems at the Institute of Transportation Studies, University of California. Through 2006, he was with TRW, Livonia, MI, USA, where he was involved in the development of advanced vehicle control systems. Since 2006, he has been faculty in the Mechanical Engineering Department, KAIST, Korea. His current research interests include fuel-saving technology, vehicle dynamics and control, and active safety systems. Prof. Choi is a Member of the American Society of Mechanical Engineers, the Society of Automotive Engineers, and the Korean Society of Automotive Engineers.